CHINESE JOURNAL OF GEOPHYSICS Vol.52, No.3, 2009, pp: 531∼540

COMPARATIVE STUDY OF SUBAURORAL POLARIZATION STREAMS WITH DMSP OBSERVATION AND RAM SIMULATION

WANG Hui[1,2,3], MA Shu-Ying[1*], RIDLEY A. J.[3]

1 *Institute of Ionosphere and Magnetosphere, LOGEG, CNME, College of Electronic Information, Wuhan University, Wuhan* 430079*, China*

2 *State Key Laboratory of Space Weather, Chinese Academy of Sciences, Beijing* 100080*, China*

3 *Department of Atmospheric, Oceanic and Space Science, University of Michigan, Ann Arbor, MI*-48105*, USA*

Abstract Subauroral Polarization Streams (SAPS) are fast westward plasma flows, located mainly at dusk and premidnight subauroral region. They are one of the important magnetosphere-ionosphere-thermosphere coupling processes. This work has simulated one storm time SAPS event with the Ring current-Atmosphere Interaction Model (RAM) developed by University of Michigan. The model results are compared with the DMSP observations. It shows: the model results can be comparable with the observations in general; the latitude of the modeled SAPS peak velocity differed greatly from the observations; the observed SAPS velocities have two peaks around 18:00 UT and 20:00 UT, while the modeled have only one peak around 18:00 UT, which is due to the model's inability in the modeling of the substorm process.

Key words Subauroral Polarization Streams, RAM model, Storm, Substorm

1 INTRODUCTION

Subauroral polarization streams (SAPS) are one of the interesting and important features of the magnetosphere-ionosphere-thermosphere coupling. They represent rapid westward (sunward) plasma flows located equatorward of the auroral oval and predominantly in the dusk and premidnight sectors (16:00∼24:00 magnetic local time (MLT)). They can change the ionospheric composition[1], lead to storm-enhanced density[2] and plasmaspheric plumes[3], produce very large field-aligned vertical flows[1], and form the F region density troughs[4].

Previous studies have reported the characteristics and morphologies of SAPS by using measurements from satellites and radars[5∼9] and from magnetospheric simulations[10∼12]. When $Kp \geq 4$ the SAPS in the premidnight sector form at 60° magnetic latitude (MLat), span 3°∼5° in latitude, and have an average peak amplitude of > 900 m/s[3]. The occurrences of SAPS are associated with substorms and storms[6,13]. The most probable local time of SAPS is found during 21:00 and 23:00 MLT, being most prominent around 22:00 MLT[14]. The magnetic latitudes of SAPS are reported to be linearly related to the magnitudes of Dst[15]. The location of SAPS is conjugate to the peak ring current energy density and the R_2 field-aligned currents (FACs)[3,7] and coincides with the equatorward edge of the ion plasma sheet[16].

The two factors that can affect the distribution of SAPS are ionospheric conductivity and R2 FACs[13]. According to the generally accepted mechanism of the SAPS formation, the enhanced convection electric field can inject more ions into the ring current and inner magnetosphere, forming a larger azimuthal pressure gradient. The stronger R2 FACs will be generated by the misalignment between the large azimuthal pressure gradient and the orientation of the magnetic field flux tube. When the large R2 FACs flows into the ionosphere region of low conductivity in the dusk sector, the electric field has to be increased to maintain the current continuity. The enhanced poleward electric field causes the SAPS to be enhanced.

This work will investigate the characteristics of SAPS during a typical magnetic storm period based on ion measurements from DMSP. The observation will be compared to RAM (Ring current-Atmosphere Interaction Model)[17] simulation, which has been developed by University of Michigan.

E-mail: h.wang@whu.edu.cn

*Corresponding author: syma@whu.edu.cn

2 DMSP DATA AND RAM MODEL

DMSP are polar orbit satellites at 835 km altitude with the orbital period of 100 minutes. The orbit plane is at fixed local time. The satellite F13 is at the dawn-dusk sector, and F15 is at 09:30∼21:30 MLT sector. The ion drift meter on board the satellite can measure the ion drift velocity that are vertical and parallel to the satellite track[18].

The RAM used in this work has been fully described by Liemohn et al.[19], which will not be detailed here. The simulation region of hot ions (energy range from 10 eV to 400 keV) in the model is $L = 1.75 \sim 6.75$, covering the whole ring current region. The pitch angle in the equatorial plane is 0°∼90°. The model solves time dependent, gyration and bounce averaged kinetic Boltzman equation,

$$\frac{\partial f^*}{\partial t}+\frac{\partial}{\partial \boldsymbol{R}_\perp}\left\{\left\langle \frac{\mathrm{d}\boldsymbol{R}_\perp}{\mathrm{d}t}_{E}\right\rangle f^*\right\}+\frac{\partial}{\partial E}\left\{\left\langle \frac{\mathrm{d}E}{\mathrm{d}t}_{E}\right\rangle f^*\right\}+\frac{\partial}{\partial \mu_0}\left\{\left\langle \frac{\mathrm{d}\mu_0}{\mathrm{d}t}_{E}\right\rangle f^*\right\}$$
$$=\frac{\partial}{\partial E}\left\{\left\langle \frac{\mathrm{d}E}{\mathrm{d}t}_{CC}\right\rangle f^*\right\}+\frac{\partial}{\partial \mu_0}\left\{\left\langle D_{CC}\right\rangle \frac{\partial f^*}{\partial t}\right\}-\frac{f^*}{\tau_{CE}}-\frac{H(\mu_0-\mu_{0,LC})f^*}{0.5\tau_b},$$

where $f(t, R, \varphi, E, \mu_0)$ is the phase-space function of a chosen ring current species, $f^* = Q \times f$, $Q = R_0^2\mu_0 h(\mu_0) \times\sqrt{E}$.

The five independent variables of $f(t, R, \varphi, E, \mu_0)$ are time (t), geocentric distance (R), magnetic local time (φ), kinetic energy (E) and cosine of pitch angle (μ_0). The left hand terms are associated with the plasma drift, including radial drift, energy and pitch angle drift et al.[19]. These terms are associated with the main phase of magnetic storm. The right hand terms are related to plasma losses and the recovery phase of magnetic storm. For example, the first two terms are related to the Coulomb collisions with the thermal plasma, the third term is related to the charge exchange with the hydrogen geocorona, the fourth term is related to the precipitation to the upper atmosphere[20].

The ion parameters at the outer simulation boundary are got from the geosynchronous satellite LANL, from which the initial distribution of ions at the outer boundary can be derived as the outer boundary condition of the kinetic function. Because the (Multiple-Particle Analyzer) MPA and (Senior Officer Present Afloat) SOPA do not resolve ion mass, the compositions of ions are determined from the statistical relationship derived by Young et al.[21] (details refer to Ref.[22]) from geosynchronous satellite measurements. The ions are convected through the simulation region by the convection electric field, magnetic gradient-curvature drifts and corotation effects. The Coulomb collisions, charge exchange and atmosphere precipitation are also included in the calculation.

In RAM, the R2 FACs can be derived from the divergence of the cross tail current[19]. Together with the ionospheric conductivity[23], the ionospheric potential can be derived through Poison function. The Weimer-96[24] convection electric field model is used at the high latitude boundary. The ionospheric conductivity includes several components, such as solar illumination, starlight and auroral particle precipitation[23]. The starlight component is set to be 1 S, the sunlight is derived using the model of Moen and Brekke[25], the auroral precipitation component is derived using an empirical statistical relationship between the R1 FACs and the conductance, which is based on AMIE (Assimilative Mapping of Ionospheric Electrodynamics)[26]. Because RAM can only calculate R2 FACs, the strength of the R1 FACs are assumed to be 5 times of R2 FACs. This assumption is based on previous statistical studies[27,28] based on satellite observations that normally R1 FACs are 5 times of R2 FACs in strength. In addition, the calculated R2 FACs peak has been shifted poleward by 5° to be the auroral oval peak. Previous studies[29] have shown that these assumptions make the simulation overall match to IMAGE EUV (Extreme Ultraviolet, plasmasphere location)and HENA (High-Energy Neutral Atom) flux observations.

The model inputs[29] include (1) the high latitude convection electric field from Weimer-96[24]. Liemohn et al.[29] have shown that this electric field model can basically describe the morphologies of the strormtime plasmasphere. In this study the Weimer-96 electric field model is still used; (2) the density, temperature, flux parameters of ions at the geosynchronous orbits, which are derived from the MPA and SOPA measurements on

board LANL combined with the empirical relationship[22]; (3) the ionospheric conductivity model[23].

The model outputs include: the phase-space distribution of hot ions (mainly hydrogen and oxygen ions), the MLT-L distribution of ion density in the equatorial plane, the MLT-L distribution of perpendicular and horizontal pressure in the equatorial plane, the MLT-L distribution of the anisotropy temperature ($T_{\rm per}/T_{\rm par}$-1) in the equatorial plane, the MLT-L distribution of energy density in the equatorial plane, the MLT-L distribution of azimuthal current in the equatorial plane, the MLT-L distribution of total ion numbers, the MLT-L distribution of ion total energy, the MLT-L distribution of electrical potential, the MLT-L distribution of total azimuthal current, total radial current, and FACs that are flowing into the ionosphere et al.. In addition, Dst index can be calculated from the total energy of ions according to the Dessler-Parker relationship[30].

3 SOLAR WIND AND IMF CONDITION

The SAPS event under study occurs on April 17 2002, which is a moderate geomagnetic storm. Fig. 1 shows the solar wind, IMF, and geomagnetic activity parameters during this magnetic storm measured by ACE satellite, which is located at Lagrange Point (L1), about 220 $R_{\rm E}$ (1.48×10^6 km) in front of the Earth. From left to right it contains the components of the IMF B_x, B_y and B_z component in GSM coordinates, Dst index, solar wind velocity, $V_{\rm sw}$, solar wind dynamic pressure, $P_{\rm d}$, merging electric field, $E_{\rm m}$[31], and Akasofu solar wind-magnetosphere coupling parameter, ε[32]. Dst arrives at a minimum value of –98 nT at 18:00 UT, the IMF B_z fluctuates a lot during the main phase of the storm, arriving at a minimum of –31 nT at 15:35 UT. At 12:00 UT the solar wind velocity arrives at a maximum of 625 km/s, the pressure arrives at a maximum of 26.2 nPa, the energy coupling parameter ε arrives at a maximum of 11×10^{12} J/s, and the merging electric field $E_{\rm m}$ arrives at a maximum of 16.1 mV/m. The SAPS event under study occurs during 18:00∼22:00 UT, which is during the recovery phase of the magnetic storm.

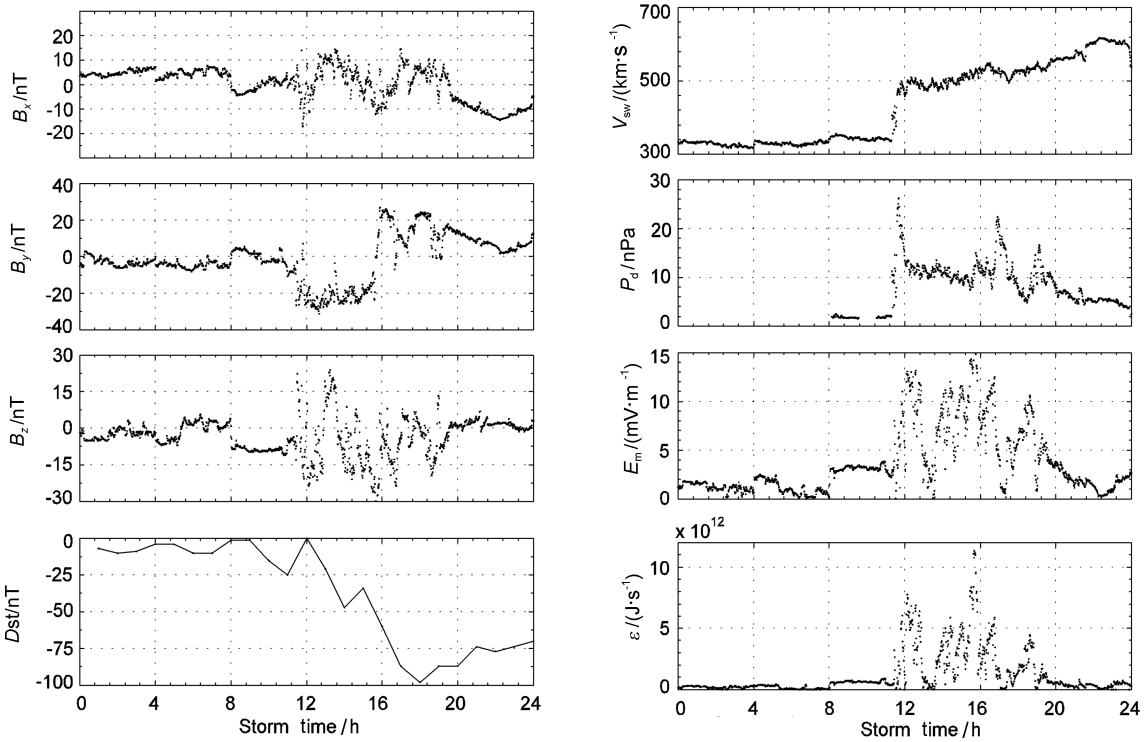

Fig. 1 The variations of IMF and solar wind, solar wind-magnetosphere coupling parameters, as well as geomagnetic indices during the moderate geomagnetic storm on 17 April 2002

4 THE COMPARISON BETWEEN OBSERVATION AND MODEL

Figure 2 shows the plasma flow velocity measured by DMSP F13 in the dusk sector in both hemispheres during 18:00∼22:00 UT. It can be seen that in the Northern Hemisphere there is a westward plasma flow with a peak velocity of 1200 m/s at 63°MLat at 18:24 UT. Similarly, there is also a westward plasma flow with a peak value of 1520 m/s at 54°MLat at 20:01 UT. In the Southern Hemisphere a strong subauroral westward plasma flow can also be observed at –55°MLat. These are all SAPS features.

Figure 3 show the plasma flow velocity modeled by RAM as a function of MLat and MLT during 18:00∼21:30 UT. It can be seen that the modeled SAPS are located in the dusk and premidnight sector around 60° MLat (indicated by dark blue). Around 18:30 UT the SAPS peak velocity arrives at a maximum value of ∼2233 m/s, then decreases gradually. The SAPS region also reduces and mainly confines around 20:00 MLT.

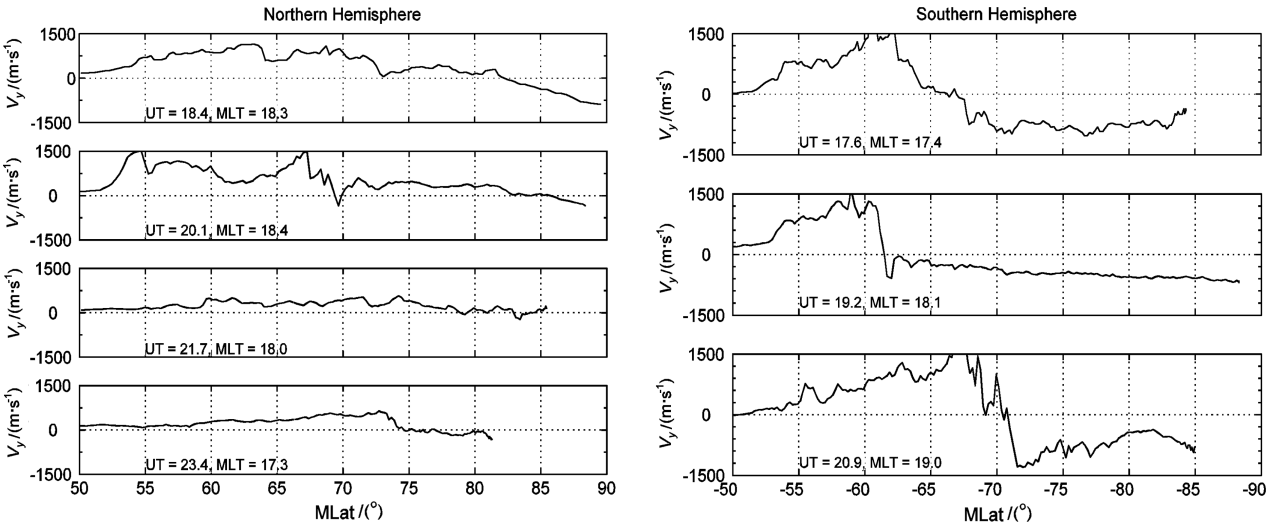

Fig. 2 The eastward and westward plasma flow velocity measured by DMSP F13 as a function of MLat
Positive (negative) denotes westward (eastward) plasma flow. Left row is the
Northern Hemisphere and right the Southern Hemisphere.

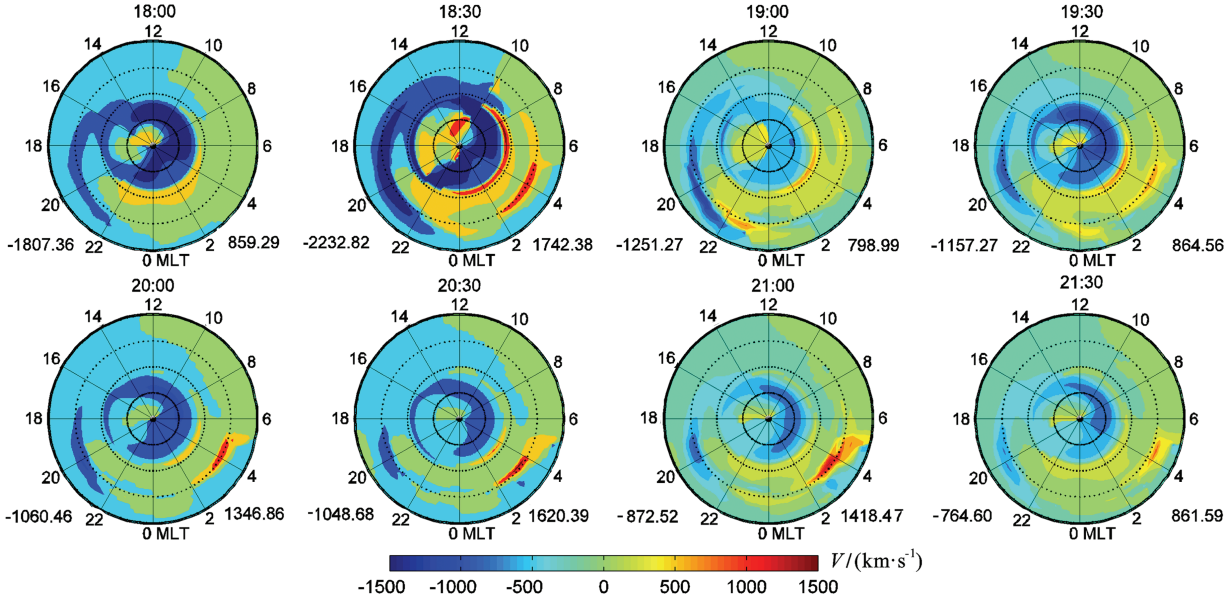

Fig. 3 The plasma flow velocity modeled by RAM as a function of MLat and MLT during 18:00 ∼ 21:30 UT
The UT interval is 30 minutes. The latitude circles from outward to inward shown are 50°, 60°, 70°, 80° MLat respectively.

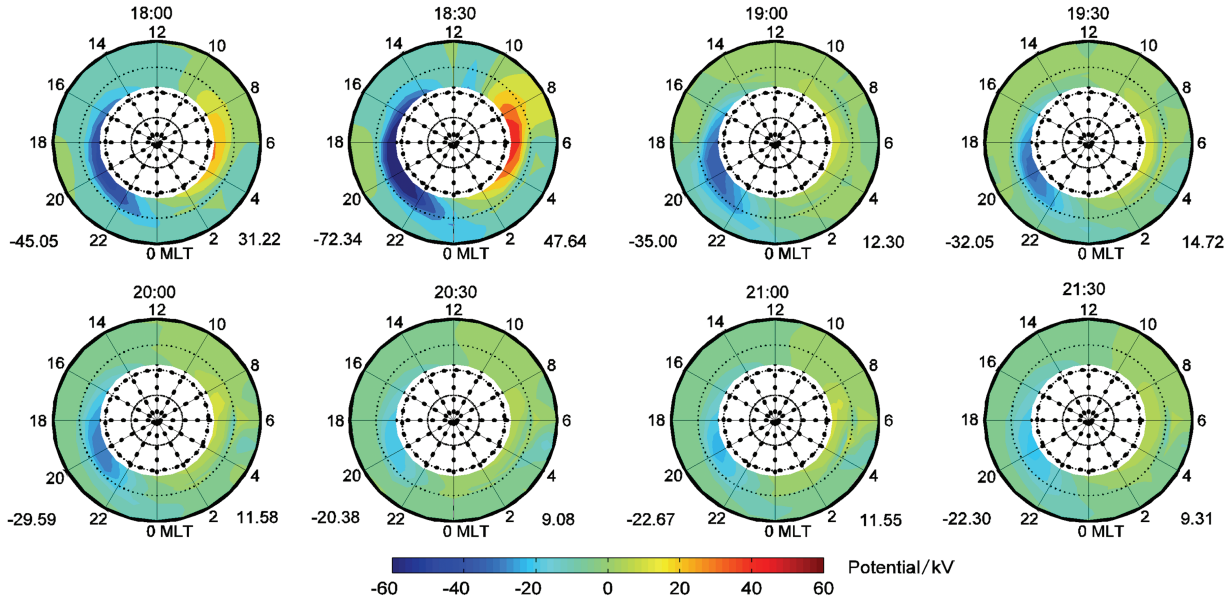

Fig. 4 The same as Fig. 3 except for the potential

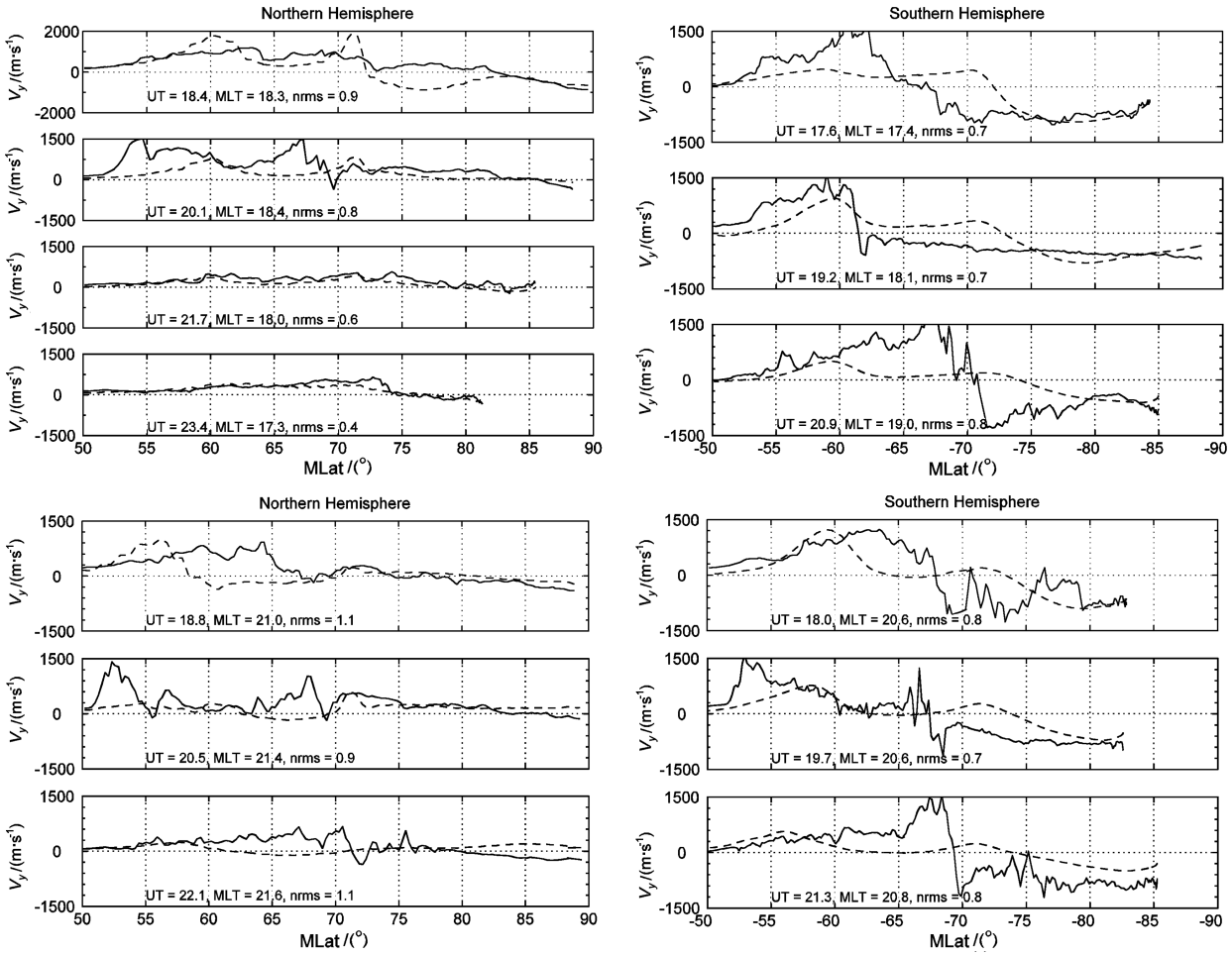

Fig. 5 The measured and modeled plasma flow velocity as a function of MLat

The above row is F13 and the bottom F15. The left column is the Northern Hemisphere and the right the Southern Hemisphere. Dashed line is the modeled value and real line the measured. The normalized root mean square (nrms) are also given.

Figure 4 shows the modeled subauroral potential distribution (the high latitude electric field is not shown). The time variations of the duskside negative potential (poleward electric field) are similar to those of the SAPS velocity. The poleward potential peaks at 18:30 UT, after that the strength gradually decreases.

Figure 5 shows the comparison between the modeled plasma velocity and the observed in the Northern Hemisphere. The dashed line is the modeled and the real line the observed. We use the normalized root mean square (nrms)[33] to evaluate the model, that is, nrms $= \sqrt{\frac{\Sigma_{i=1}^{n}(y_i - y_i^*)^2}{\Sigma_{i=1}^{n} y_i^2}}$, where y_i is the observed, y_i^* is the modeled value. nrms=0 means that the modeled value is equal to the observed. If the model is higher than the observation, or they just have the opposite trends, nrms> 1. It can be seen that the modeled match more to F13 observations than to F15, which is consistent with our previous result that the model performs better in the duskside than in the midnight[33].

The model and the observation both show that the SAPS velocity is stronger around 18:00 UT. The observation also shows that the SAPS velocity is stronger around 20:00 UT, which is not shown in the model. From the observations it can be seen that SAPS shift towards low latitude during 19:30∼20:30 MLT while the modeled SAPS latitude does not show such large variations.

Figure 6 show the measured and modeled plasma peak flow velocity and their MLat as a function of UT. The dashed line is the modeled and the real line is the observed. It can be seen that before 20:00 UT the modeled is larger than the observed, after that the modeled is smaller than the observed. The modeled SAPS latitude does not show large variations, at 59°MLat in the duskside, at 57°MLat in the premidnight. The observed SAPS show large variations in latitude, during 18:30∼20:30 UT the observed shift equatorward by about 5°.

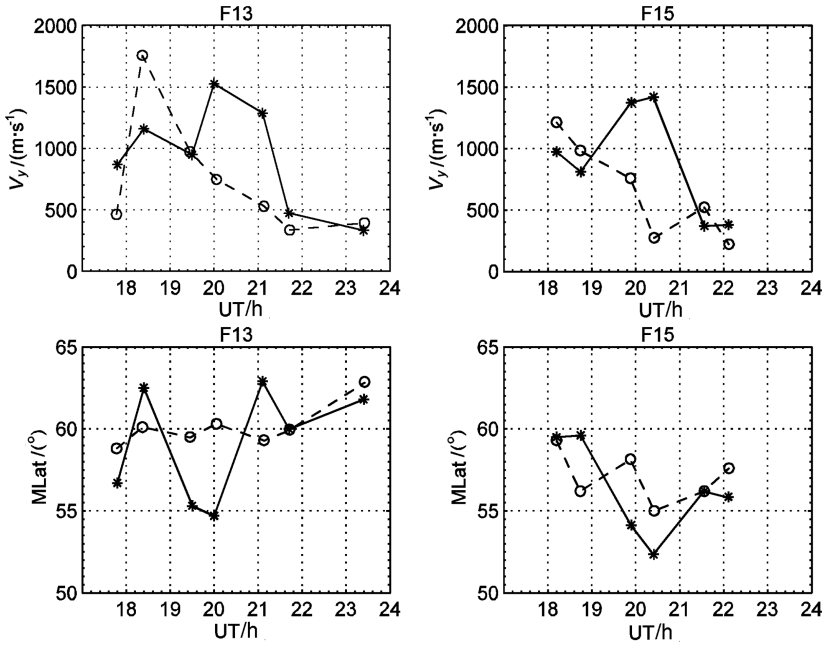

Fig. 6 The measured and modeled plasma peak flow velocity as well as their MLat as a function of UT
Dashed line denotes the modeled value and real line the measured.

5 DISCUSSION AND CONCLUSION

This study has simulated one SAPS event during a typical storm period by using RAM model developed by University of Michigan. The results have been compared with DMSP observations. Previous work has validated RAM in certain aspects. For example, some work has compared RAM with IMAGE EUV images (plasmasphere location), HENA (High-Energy Neutral Atom) flux images (39∼60 keV energy) as well as *D*st

index (ring current strength)[11,29,34], but the validation of the subauroral polarization streams of RAM has not been done before.

Subauroral polarization streams are one of the important features in the inner magnetosphere-ionosphere-thermosphere coupling. They are associated with R2 FACs, ring currents and ionspheric polarization electric field. During high geomagnetic activity, stronger polarization electric field can be observed equatorward of the electron boundary of the plasma sheet and poleward of the ion boundary of the plasmasheet in the nightside. At duskside ions in the plasma sheet move more near the Earth than electrons. It is known that ions are the main carrier of R2 FACs. Therefore, R2 FACs will flow into the subauroral region with low ionospheric conductivity. The electric field has to increase to maintain the current continuity. The enhanced poleward electric field will enhance the westward plasma flow (SAPS). In RAM, the ionospheric electric field is determined from both ion distribution in the plasma sheet and ionospheric conductivity[11], thus, it is important to know the goodness of the model in simulating SAPS, which is important for the whole evaluation of the model performance.

This work has compared the observed and modeled SAPS to enable users of the model to know the limitation of the model. Through the validation of the model, users can get advices and suggestions for the model improvement.

The model can reflect the basic SAPS features, but show large differences in details. The satellites observe two peaks, around 18:00∼18:30 UT and 19:30∼20:00 UT, but RAM only see one peak during 18:00∼18:30 UT. Previous studies have shown that the strength of ring current is mainly controlled by the high latitude convection electric field[35∼37], therefore, it can be expected that the SAPS velocity is also affected by the high latitude convection electric field. On the other hand, the substorm particle injection can also affect the strength of the ring current[38]. The substorm polarization can drive the plasmasphere ion sunward (westward) move, thus causing the SAPS velocity enhancement. To study these two processes (convection electric field and substorm) influence on the SAPS, Fig. 7 shows the AMIE produced CPCP and AL index variations with time. The global magnetometer data, the available interplanetary magnetic field, solar wind, hemispheric power index, $F_{10.7}$, and Dst data are used as inputs into the AMIE model (See Ref.[39]). It can be seen from Fig. 7 that CPCP has two peaks of 150 kV and 110 kV, which is the same as the observed SAPS peaks (18:00∼18:30 UT and 19:30∼20:00 UT). The second peak is smaller than the first, which contradicts with the fact that the second observed SAPS velocity is larger than the first one. AL index has one peak during 19:30∼20:00 UT, which is in correspondence to the second observed SAPS peak. The analysis shows that RAM model has some limitation in the modeling of the substorm process, thus, it can not model the second peak of SAPS.

The convection electric field at the outer boundary is given by Weimer-96[24]. Liemohn et al.[29] have compared three ionospheric electric field models that may affect the RAM performance and thought that Weimer-96[24] model can make RAM predict well stormtime plasmasphere morphology, thus we use this electric field model in this study.

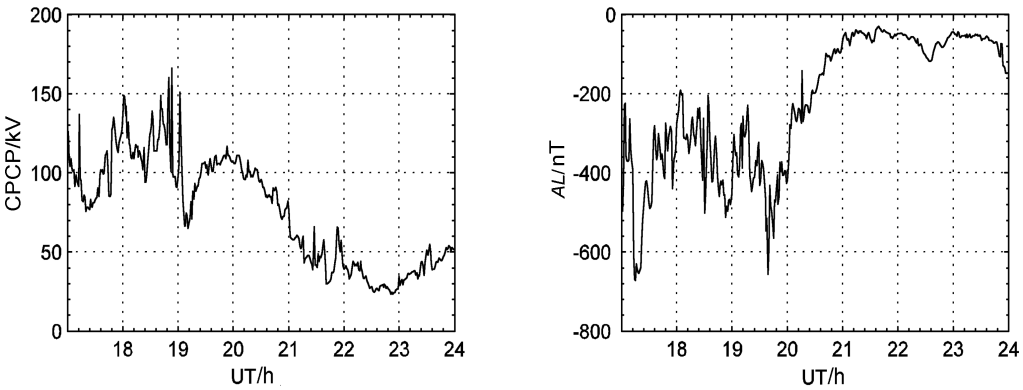

Fig. 7 AMIE output high latitude CPCP and AL index as a function of UT

The outer boundary of RAM is at geosynchronous ($\sim 6R_{\rm E}$), which is innerward of the substorm ion injection boundary ($\sim 6R_{\rm E}$ $\sim 8R_{\rm E}$), thus, in RAM the plasma is driven into the simulation region only by the convection electric field. It has been a long time that the literature has large disputes about whether the substorm can contribute to the stormtime ring current development or to the component changes[40,41]. For example Fok et al.[42] have shown that substorm dipolarization process can not inject ions into inner magnetosphere, the strong convection electric field must also exist to help transfer, then the ring current strength can be enhanced. However, some experts have different ideas[43]. On the other hand, other experts thought that only ions with energy low than 50 keV can convect through the ring current region[44]. Substorm normally increase ions energy above 50 keV[45]. These high energy ions convect from the nightside to the dayside, finally slip away from the magnetosphere and lose off, can not arrive the ring current region, thus will not affect the formation of the ring current. Even it has some effects, it will not be too much.

The present study has shown that with small convection electric field the substorm can enhance the SAPS strength. Since SAPS strength is proportional to R2 FACs, and the latter is proportional to the ring current pressure, the present results show that substorm has important effects on the development of the ring current, which is consistent with the results of Anderson et al.[43].

Like many other empirical electric field models, Weimer-96 convection electric field model lacks of the nightside processes, that is, the influence of the substorm on the nightside electric field. Since substorm has important effect on the ionospheric electric field, we must include the substorm component in the SAPS simulation, Weimer[46] also show that only using solar wind IMF as inputs as done in the Weimer-96[24], it can not describe the substorm time ionospheric convection electric field. The present work shows that substorm is important in the development of SAPS by comparing the RAM model with DMSP observation. Thus, it is important to improve the high latitude convection electric field model. Weimer-2001 convection electric field model has made such improvements based on Weimer-96, which has added *AL* index as inputs. Weimer has used this new electric field model to simulate one substorm event and found that the model results can reflect the observations quite well[46]. Thus our next work will consider Weimer-2001[46] in stead of Weimer-96[24], to expect the results to get improved.

The latitudes of SAPS peak velocities has large variations around 20:00 UT (after substorm), SAPS peaks shift towards equatorward by at least 5°, while the simulated SAPS peak velocities has no big changes, which is due to the RAM model's inability in modeling the substorm process. On the other hand, the difference between the modeled and observed latitude of the SAPS peak velocities is related to the aurora location in the ionospheric conductivity models. In the model we suppose that the peak aurora is 5° poleward of the peak R2 FACs, but in reality this difference can change with the storm time. The latitude of SAPS peak velocities coincide with the peak of R2 FACs and ring current, the difference between the modeled and observed SAPS indicates that the modeled R2 FACs and ring currents have also errors.

ACKNOWLEDGMENTS

The RAM and AMIE model used in the present work are provided by CSEM at University of Michigan, ACE satellite data and various magnetic field indexes are provided by ISTP PI through internet. We thanks Prof. Liemohn at UM for helpful discussion. This work is supported by the National Nature Science Foundation of China (40604017) and the specialized research fund for state key laboratories.

REFERENCES

[1] Anderson P C, Heelis R A, Hanson W B. The ionospheric signatures of rapid subauroral ion drifts. *J. Geophys. Res.*, 1991, **96**(A4): 5785∼5792

[2] Foster J C, Rideout W. Storm enhanced density: magnetic conjugacy effects. *Ann. Geophys.*, 2007, **25**: 1791∼1799

[3] Foster J C, Vo H B. Average characteristics and activity dependence of the subauroral polarization stream. *J. Geophys. Res.*, 2002, **107**(A12): doi: 10.1029/2002JA009409

[4] Spiro R W, Heelis R A, Hanson W B. Ion convection and the formation of the mid-latitude F region ionization trough. *J. Geophys. Res.*, 1978, **83**(A9): 4255∼4264

[5] Galperin Y, Ponomarev V N, Zosimova A G. Plasma convection in the polar ionosphere. *Ann. Geophys.*, 1974, **30**(1): 1∼7

[6] Spiro R W, Heelis R H, Hanson W B. Rapid sub-auroral ion drifts observed by Atmospheric Explorer C. *Geophys. Res. Lett.*, 1979, **6**(8): 657∼660

[7] Yeh H -C, Foster J C, Rich F J, et al. Storm time electric field penetration observed at mid-latitude. *J. Geophys. Res.*, 1991, **96**(A4): 5707∼5721

[8] Jensen J W, Fejer B G. Longitudinal dependence of middle and low latitude zonal plasma drifts measured by DE-2. *Ann. Geophys.*, 2007, **25**(12): 2551∼2559

[9] Wang H, Ridley A J, Luehr H, et al. Statistical study of the subauroral polarization streams: its dependence on the cross polar cap potential and subauroral conductance. *J. Geophys. Res.*, 2008, doi: 10.1029/2008JA013529

[10] Garner T W, Wolf R A, Spiro R W, et al. Magnetospheric electric fields and plasma sheet injection to low L-shells during the 4-5 June 1991 magnetic storm: comparison between the Rice Convection Model and observations. *J. Geophys. Res.*, 2004, **109**(A02214): doi: 10.1029/2003JA010208

[11] Liemohn M W, Ridley A J, Brandt P C, et al. Parametric analysis of nightside conductance effects on inner magnetospheric dynamics for the 17 April 2002 storm. *J. Geophys. Res.*, 2005, **110**(A12): doi: 10.1029/2005JA011109

[12] Zheng Y, Brandt P C, Lui A T, et al. On ionospheric trough conductance and subauroral polarization streams: simulation results. *J. Geophys. Res.*, 2008, **113**(A04): doi: 10.1029/2007JA012532

[13] Anderson P C, Hanson W B, Heelis R A, et al. A proposed production model of rapid subauroral ion drifts and their relationship to substorm evolution. *J. Geophys. Res.*, 1993, **98**(A4): 6069∼6078

[14] Karlsson T, Marklund G T, Blomberg L G. Subauroral electric fields observed by the Freja satellite: a statistical study. *J. Geophys. Res.*, 1998, **103**(A3): 4327∼4341

[15] Huang C -S, Foster J C. Correlation of the subauroral polarization streams (SAPS) with the *D*st index during severe magnetic storms. *J. Geophys. Res.*, 2007, **112**(A11302): doi: 10.1029/2007JA012584

[16] Southwood D J, Wolf R A. An assessment of the role of precipitation in magnetospheric convection. *J. Geophys. Res.*, 1978, **83**(A11): 5227∼5232

[17] Fok M -C, Koyra J U, Nagy A F, et al. A decay model of equatorial ring current and the associated aeronomical consequences. *J. Geophys. Res.*, 1993, **98**(A11): 19381∼19393

[18] Rich F J, Hairston M. Large-scale convection patterns observed by DMSP. *J. Geophys. Res.*, 1994, **99**(A3): 3827∼3844

[19] Liemohn M W, Kozyra J U, Thomsen M F, et al. Dominant role of the asymmetric ring current in producing the stormtime *D*st. *J. Geophys. Res.*, 2001, **106**(A6): 10883∼10904

[20] Jordanova V K, Kistler L M, Kozyra J U, et al. Collisional losses of ring current ions. *J. Geophys. Res.*, 1996, **101**: 111∼126

[21] Young D T, Balsiger H, Geiss J. Correlations of magnteospheric ion composition with geomagnetic and solar activity. *J. Geophys. Res.*, 1982, **87**(A11): 9077∼9096

[22] Liemohn M W, Kozyra J U, Jordanova V K, et al. Analysis of early phase ring current recovery mechanisms during geomagnetic storms. *Geophys. Res. Lett.*, 1999, **26**: 2845∼2848

[23] Ridley A J, Gombosi T I, DeZeeuw D L. Ionospheric control of the magnetosphere: conductance. *Ann. Geophys.*, 2004, **22**: 567∼584

[24] Weimer D R. A flexible IMF dependent model of high-latitude electric potentials having "space weather" applications. *Geophys. Res. Lett.*, 1996, **23**: 2549∼2552

[25] Moen J, Brekke A. The solar flux influence on quiet time conductances in the auroral ionosphere. *Geophys. Res. Lett.*, 1993, **20**(10): 971∼974

[26] Ahn B -H, Richmond A D, Kamide Y, et al. An ionospheric conductance model based on ground magnetic disturbance data. *J. Geophys. Res.*, 1998, **103**(A7): 14769∼14780, doi: 10.1029/97JA03088

[27] Iijima T, Potemra T A. The amplitude distribution of fieldaligned currents at northern latitudes observed by TRIAD. *J. Geophys. Res.*, 1976, **81**: 2165∼2174

[28] Wang H, Lühr H, Ma S Y. Solar zenith angle and merging electric field control of field-aligned currents: a statistical study of the Southern Hemisphere. *J. Geophys. Res.*, 2005, **110**(A03306): doi:10.1029/2004JA010530

[29] Liemohn M W, Ridley A J, Gallagher D L, et al. Dependence of plasmaspheric morphology on the electric field description during the recovery phase of the 17 April 2002 magnetic storm. *J. Geophys. Res.*, 2004, **109**(A03209): doi:10.1029/2003JA010304

[30] Dessler A J, Parker E N. Hydromagnetic theory of geomagnetic storms. *J. Geophys. Res.*, 1959, **64**: 2239∼2252

[31] Kan J R, Lee L C. Energy coupling function and solar wind magnetosphere dynamo. *Geophys. Res. Lett.*, 1979, **6**: 577∼580

[32] Akasofu S I. Interplanetary energy flux associated with magnetospheric substorms. *Planet. Space. Sci.*, 1979, **27**: 425∼431

[33] Wang H, Ridley A J, Luehr H. Validation of the SpaceWeather Modeling Framework with observations from DMSP and CHAMP. *Space Weather*, 2008, **6**(S03): doi: 10.1029/2007SW000355

[34] Kozyra J U, Liemohn M W. Ring current energy input and decay. *Space Sci. Rev.*, 2003, **109**: 105∼131

[35] Daglis I A, Kozyra J U. Outstanding issues of ring current dynamics. *J. Atmos. Solar-Terr. Phys.*, 2002, **64**: 253∼264

[36] Fu S Y, Zong Q G, Pu Z Y, et al. Effect of geomagnetic activity and solar-cycle variation on the ring current ions. *Chinese J. Geophys.* (in Chinese), 2003, **46**(6): 725∼730

[37] Xie L, Pu Z Y, Zhou X Z, et al. Formation of the storm-time ring current. *Chinese Science Bulletin* (in Chinese), 2004, **49**(7): 716∼723

[38] Ganushkina N Y, Pulkkinen T I, Bashkirov V F, et al. Formation of intense nose structures. *Geophys. Res. Lett.*, 2001, **28**(3): 491∼494

[39] Ridley A J, Kihn E A. Polar cap index comparisons with AMIE cross polar cap potential, electric field, and polar cap area. *Geophys. Res. Lett.*, 2004, **31**(L07801): doi: 10.1029/2003GL019113

[40] Kamide Y, Baumjohann W, Daglis I A, et al. Current understanding of magnetic storms: storm-substorm relationships. *J. Geophys. Res.*, 1998, **103**: 17705∼17728

[41] Gonzalez W D, Joselyn J A, Kamide Y, et al. What is a geomagnetic storm? *J. Geophys. Res.*, 1994, **99**: 5771∼5792

[42] Fok M C, Moore T E, Delcourt D C, et al. Modeling of inner plasma sheet and ring current during substorms. *J. Geophys. Res.*, 1999, **104**: 14557∼14569

[43] Anderson P C, Hanson W B, Heelis R A, et al. A proposed production model of rapid subauroral ion drifts and their relationship to substorm evolution. *J. Geophys. Res.*, 1993, **98**(A4): 6069∼6078

[44] Liemohn M W, Kozyra J U. Lognormal form of the ring current energy content. *J. Atmos. Solar-Terr. Phys.*, 2003, **65**(5): 871∼886

[45] Birn J, Thomsen M F, Borovsky J E, et al. Characteristic plasma properties during dispersionless substorm injections at geosynchronous orbit. *J. Geophys. Res.*, 1997, **102**: 2309∼2324

[46] Weimer D R. An improved model of ionospheric electric potentials including substorm perturbations and application to the Geospace Environment Modeling November 24, 1996, event. *J. Geophys. Res.*, 2001, **106**: 407∼416